Electronic Supplementary Material (ESI) for Journal of Materials Chemistry C.
This journal is © The Royal Society of Chemistry 2022

Supporting Information

Mechanical, electronic and photocatalytic properties of binary Ge-based materials GeX_2 (X = B, C, N) with pentagonal structure

Jiajia Liu,[1†] Yanqing Shen,[1,2*†] Lingling Lv,[1] Xianghui Meng,[1] Xu Gao,[1] Min Zhou,[1] XinYang,[1] Yu Zhang,[1] Yangdong Zheng,[1,2] Zhongxiang Zhou[1,2]

1 School of Physics, Harbin Institute of Technology, Harbin 150001, PR China

2 Heilongjiang Provincial Key Laboratory of Plasma Physics and Application Technology, Harbin Institute of Technology, Harbin 150001, PR China

* Corresponding author: Yanqing Shen. E-mail: shenyanqing2004@163.com

† These authors contributed equally to this work

1. Structural parameters of the predicted *penta*-GeX_2 (X = B, C, N)

Table S1. Structural information of the predicted *penta*-GeX_2 (X = B, C, N) monolayers

Phase	Space Group	Lattice Parameters (Å, °)		Atoms	Wyckoff Positions		
					x	*y*	*z*
penta-GeB_2	$P2_1m$	a = 5.08	α = 90.00	Ge	0.000	0.000	0.000
		b = 5.08	β = 90.00	B	0.116	0.616	0.021
		c = 20.00	γ = 90.00				
penta-GeC_2	$P2_1m$	a = 4.56	α = 90.00	Ge	0.000	0.000	0.000
		b = 4.56	β = 90.00	C	0.104	0.604	0.284
		c = 20.00	γ = 90.00				
penta-GeN_2	$P2_1m$	a = 4.26	α = 90.00	Ge	0.000	0.000	0.000
		b = 4.26	β = 90.00	N	0.122	0.622	0.261
		c = 20.00	γ = 90.00				

2. Different configurations of GeX_2 (X = B, C, N)

To demonstrate that this particular structural model yields the lowest-energy configurations of these compounds, we calculated different configurations of GeX_2 (X=B, C, N). They are *penta*-GeX_2, *orthor*-GeX_2, *cubicubic*-GeX_2, and *tetrahex*-GeX_2, as shown in Fig. S1. We compared the lowest energies of different structures by optimizing the structure and calculating the cohesive energy, and the results are listed in Table S2.

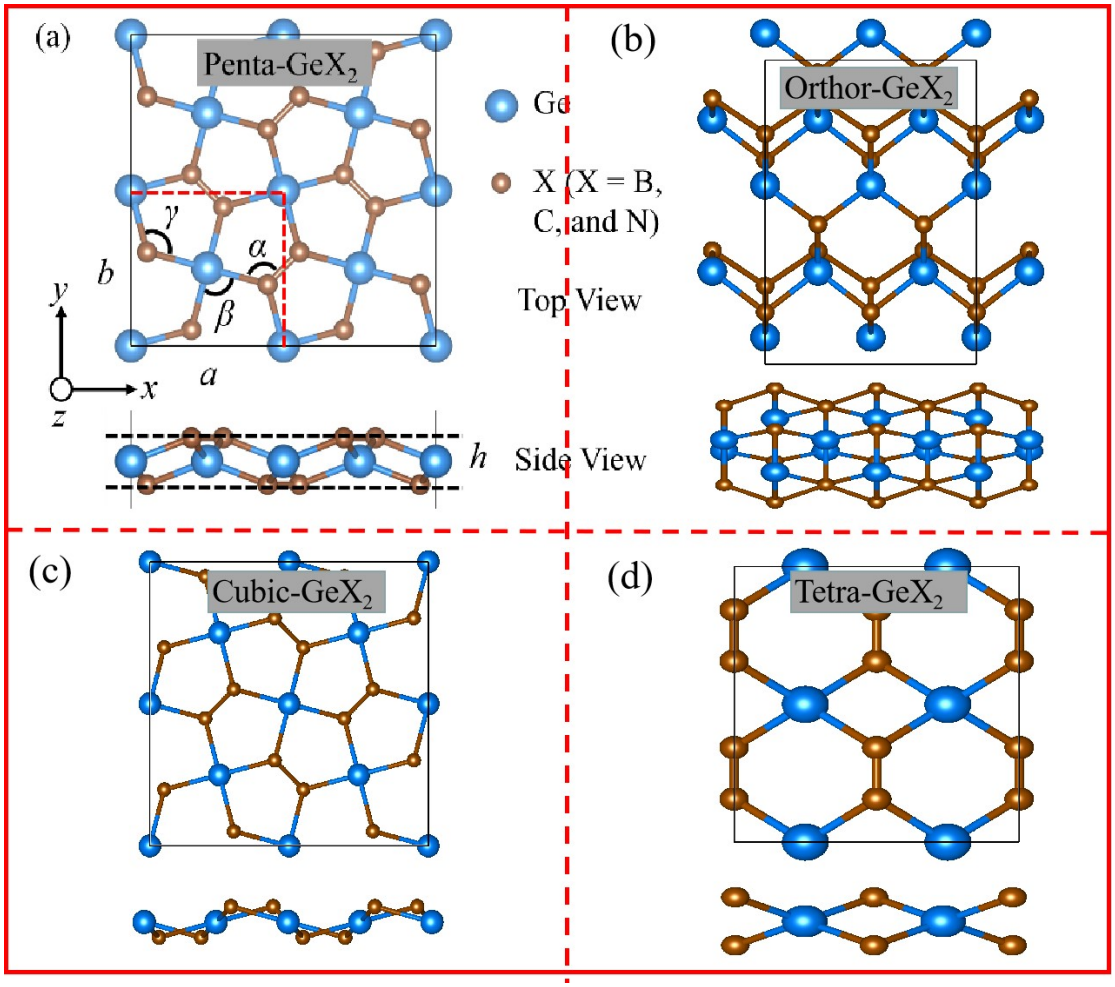

Fig. S1 The different configurations of GeX_2 (X=B, C, N). (a) *penta*-GeX_2, (b) *orthor*-GeX_2, (c) *cubicubic*-GeX_2, and (d) *tetrahex*-GeX_2.

Table S2. The cohesive energy of *penta*-GeX_2, *orthor*-GeX_2, *cubicubic*-GeX_2, and *tetrahex*-GeX_2 monolayers.

Structure type	GeB_2 (eV/atom)	GeC_2 (eV/atom)	GeN_2 (eV/atom)
penta-phase	-4.27	-5.81	-3.96
orthor-phase	-3.92	——	——
cubicubic-phase	-4.27	-5.81	-3.96
tetrahex-phase	——	-5.52	-3.83

It can be seen from Table S2 that only *orthor*-GeB_2 in the *orthor*-GeX_2 structure is thermodynamically stable. Its formation energy is -3.92 eV/atom, which is much lower than that of *penta*-GeB_2 (-4.27 eV/atom)。*Cubic*-GeX_2 has the same cohesive energy as *penta*-GeX_2, because *cubic*-GeX_2 undergoes structural change after structural

relaxation to form *penta*-GeX_2, which further verifies that *penta*-GeX_2 has the lowest energy configuration. Finally, for tetrahex-GeX_2, the cohesive energy of *tetrahex*-GeC_2 was previously reported in relevant literature (-5.50 eV/atom)[1] (*ACS Appl. Mater. Interfaces* **2021**, 13, 12, 14489–14496), which is consistent with the -5.52 eV/atom energy calculated in this manuscript, indicating the reliability of our calculations. However, the cohesive energies of *tetrahex*-GeC_2 and *tetrahex*-GeN_2 are still lower than those of *penta*-GeC_2 and *penta*-GeN_2. Therefore, considering the different structures of GeX_2, the *penta*-GeX_2 (X = B, C, N) model yields the lowest energy configurations of these compounds.

3. K-points convergence test

We tested the K-points calculation parameters, and the results are shown in Fig. S2. As the K point increases, the energy gradually converges. When the K-points is 5x5x1, the system energy no longer changes as the K point increases. Fig. S2 also reflects the relationship between the increase of K-points and the time consumed by the calculation. It can be seen from the figure that when the K-points reach 5x5x1, continuing to increase the K point will only consume more time. Therefore, when we calculate the structure optimization using 5x5x1 K-points, the energy convergence criterion is satisfied and the time consumption is the shortest.

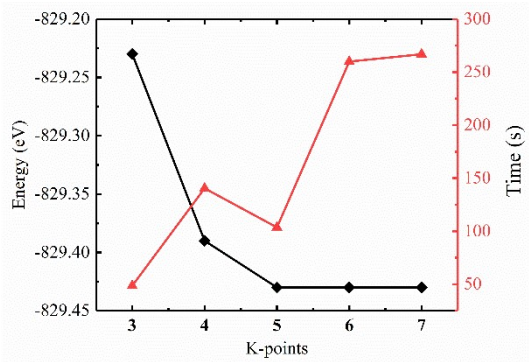

Fig. S2 K-point convergence test. The relationship between the system energy and the time used in the calculation varies with the K point.

4. Independent elastic constants

There are 3 independent elastic constants for *penta*-GeX_2 (X = B, C, N) monolayers.

$$C = \begin{bmatrix} C_{11} & C_{12} & 0 \\ C_{12} & C_{22} & 0 \\ 0 & 0 & C_{66} \end{bmatrix}$$

We obtain for the *penta*-GeB_2 monolayer:

$$C = \begin{bmatrix} 96.74 & 38.96 & 0 \\ 38.96 & 96.74 & 0 \\ 0 & 0 & 8.09 \end{bmatrix}$$

We obtain for the *penta*-GeC_2 monolayer:

$$C = \begin{bmatrix} 175.58 & 49.22 & 0 \\ 49.22 & 175.58 & 0 \\ 0 & 0 & 22.10 \end{bmatrix}$$

We obtain for the *penta*-GeN_2 monolayer:

$$C = \begin{bmatrix} 187.31 & 41.06 & 0 \\ 41.06 & 187.31 & 0 \\ 0 & 0 & 27.11 \end{bmatrix}$$

Table S3 Calculated in-plane stiffness constants C_{ij}, Young's modulus Y, and Poisson's ratio v of penta-GeX_2 (X = B, C, N), respectively

	$C_{11}=C_{22}$	C_{12}	C_{66}	Y ($Y_x=Y_y$)	v ($v_x=v_y$)
penta-GeB_2	96.74	38.96	8.09	81.05	0.40
penta-GeC_2	175.58	49.22	22.10	161.78	0.28
penta-GeN_2	187.31	41.06	27.11	178.31	0.22

5. Band structure with PBE and HSE functional

The band diagrams calculated using the PBE functional and the HSE hybrid functional, which we have added in the supplementary material. As shown in Figure S3 below, the band types of the three structures are unchanged, but the size of the band gap value has changed. It is well known that the PBE functional generally underestimates the value of the band gap of semiconductors, and the band gap is significantly corrected after using the hybrid functional.

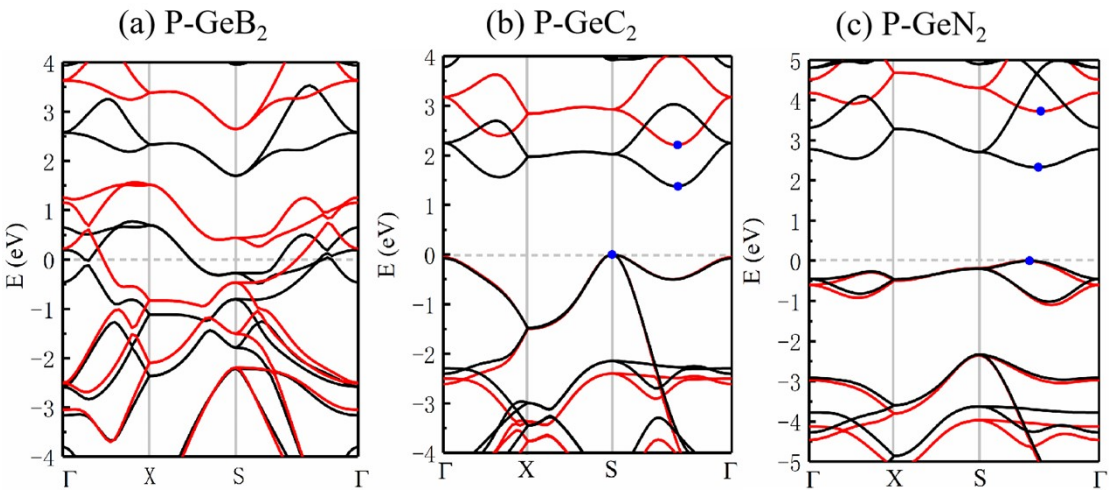

Fig. S3 Band structure of the (a) *penta*-GeB_2, (b) *penta*-GeC_2, and (c) *penta*-GeN_2 monolayers calculated by the PBE and HSE06 functional. (The black and red lines represent band structures calculated by PBE and HSE functional, respectively.)

Table S4 The band gaps E_g (in eV) at PBE and HES06 levels, position of CBM and VBM relative to the vacuum level of penta-GeX2 (X = C, N) monolayers at the HSE06 level.

	E_g^{PBE}	E_g^{HSE06}	CBM (vs. E_{vac})	VBM (vs. E_{vac})	
penta-GeC_2	1.57	2.39	-3.81	-6.19	indirect
penta-GeN_2	2.33	3.73	-3.62	-7.35	indirect

6. Carrier mobility

The following formula was used to define the 2D carrier mobility:[2,3]

$$\mu_{2D} = \frac{e\hbar^3 C_{2D}}{k_B T m^* m_d E_d^2} \qquad \text{S(1)}$$

in which e is the electron charge, $\hbar$ is Planck's constant divided by 2π, k_B is Boltzmann's constant, and T is temperature set to be 300 K. m^* is the effective mass of electron or hole, which can be calculated from the derivatives of electronic bands using the formula:

$$m^* = \hbar^2 \left[\frac{\partial^2 E(k)}{\partial k^2} \right]^{-1} \qquad \text{S(2)}$$

where k and $E(k)$ are the wave vector and the energy corresponding to k, respectively. m_d is the average effective mass defined by $m_d = \sqrt{m_x^* m_y^*}$. C_{2D} is the elastic modulus of

the 2D system along the transport direction, and is set by

$$C_{2D} = \frac{1}{S_0}\left[\frac{\partial^2 E}{\partial \delta^2}\right] \quad \text{S(3)}$$

wherein the strain δ is determined by $\Delta l / l_0$ (Δl is the change of the lattice parameter, and l_0 is the equilibrium lattice parameter). E and S_0 represent total energy and pristine superficial area, respectively. The E_d is the deformation potential constant, which indicates the shift of band edges by the strain. The expression is shown as follow:

$$E_{\mathrm{d}} = \frac{\partial E_{\mathrm{edge}}}{\partial \delta} \quad \text{S(4)}$$

e, T, $\hbar$, and k_B represent electron charge, temperature (300 K), reduced Planck constant, and Boltzamann constant, respectively.

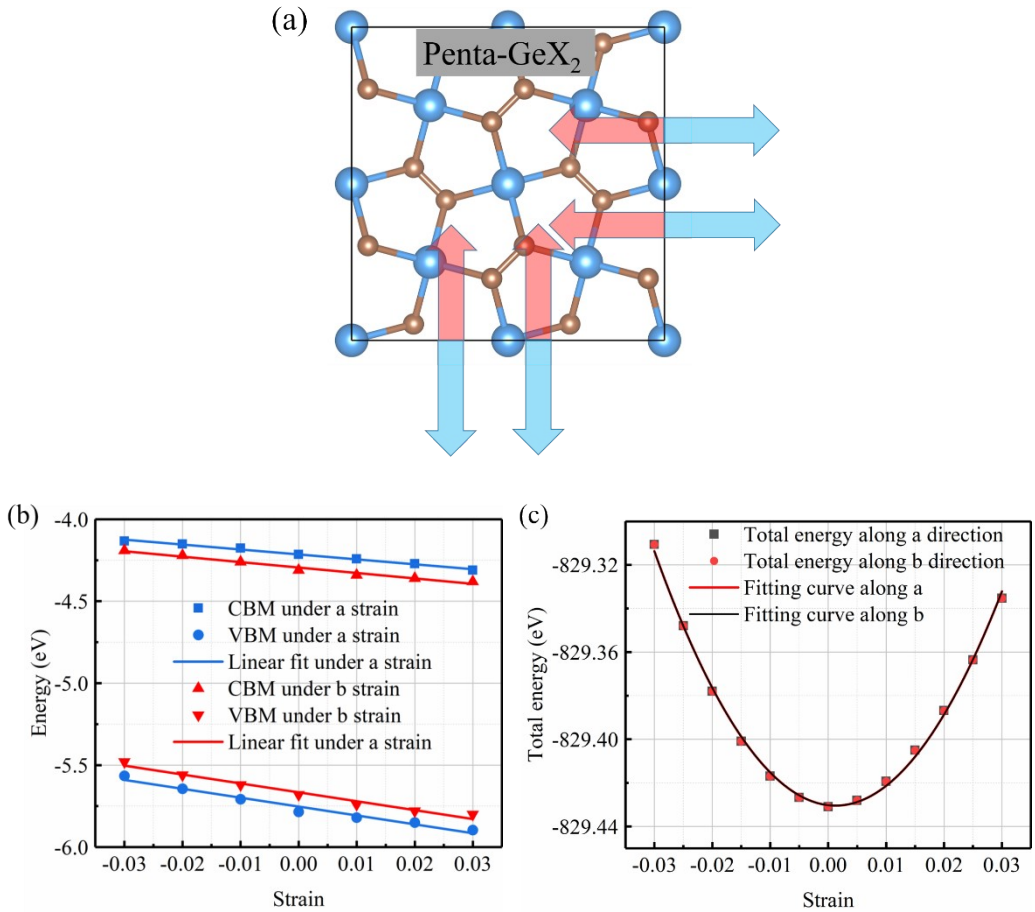

Fig. S4 (a) schematic of strain. (b) Shift of band edge (CBM and VBM) under the strain along *a* and *b* directions and (c) the total energy change under the strain along *a* and *b* directions.

7. Gibbs free energy calculations

In aqueous solution, the HER process generally can be decomposed into two steps, which can be expressed as follows

$$* + \mathrm{H}^+ + e^- \rightarrow \mathrm{H}^* \qquad \mathrm{S}(5)$$

$$\mathrm{H}^* + \mathrm{H}^+ + e^- \rightarrow * + \mathrm{H}_2 \qquad \mathrm{S}(6)$$

while for the OER process, the half reaction can be decomposed into four steps, each step provides a proton and an electron:[4]

$$\mathrm{H_2O} + * \rightarrow \mathrm{OH}^* + e^- + \mathrm{H}^+ \qquad \mathrm{S}(7)$$

$$\mathrm{OH}^* \rightarrow \mathrm{O}^* + e^- + \mathrm{H}^+ \qquad \mathrm{S}(8)$$

$$\mathrm{H_2O} + \mathrm{O}^* \rightarrow \mathrm{OOH}^* + e^- + \mathrm{H}^+ \qquad \mathrm{S}(9)$$

$$\mathrm{OOH}^* \rightarrow * + \mathrm{O_2} + e^- + \mathrm{H}^+ \qquad \mathrm{S}(10)$$

where * is the active site on the photocatalysts, O*, OH*, OOH* and H* represent the intermediates of reactions.

We calculated the Gibbs free energy change ΔG which proposed by Nørskov *et al.*[5] defined as

$$\Delta G = \Delta E + \Delta E_{ZPE} - T\Delta S + \Delta G_U + \Delta G_{PH} \qquad \mathrm{S}(11)$$

here, ΔE represents the DFT energy difference between the free standing and adsorbed states of reaction intermediates, ΔE_{ZPE} and TΔS are the zero-point energy difference and the entropy, respectively. $\Delta G_U = -eU$ is the relevant electrode potential U. ΔG_{pH} represents the Gibbs free energy which was corrected to H^+ concentrations.

Then, the ΔG under the effect of electrolyte pH were achieved as:

$$\Delta G_{H^*} = G_{H^*} - 1/2\, G_{H_2} - G^* + 0.059 \times pH - eU \qquad \mathrm{S}(12)$$

$$\Delta G_{OH^*} = G_{OH^*} + 1/2\, G_{H_2} - G_{H_2O} - G^* - 0.059 \times pH - eU \qquad \mathrm{S}(13)$$

$$\Delta G_{O^*} = G_{O^*} + 1/2\, G_{H_2} - G_{OH^*} - 0.059 \times pH - eU \qquad \mathrm{S}(14)$$

$$\Delta G_{OOH^*} = G_{OOH^*} + 1/2\, G_{H_2} - G_{H_2O} - G_{O^*} - 0.059 \times pH - eU \qquad \mathrm{S}(15)$$

$$\Delta G_{O_2} = G^* + 1/2\, G_{H_2} + G_{O^2} - G_{OOH^*} - 0.059 \times pH - eU \qquad \mathrm{S}(16)$$

where 0.059 × *pH* is the free energy contribution under the effect of pH, *eU* represent

the influence of extra potential bias provided the electrons and holes in the electrode, and U is the external potential relative to the standard hydrogen electrode (SHE).

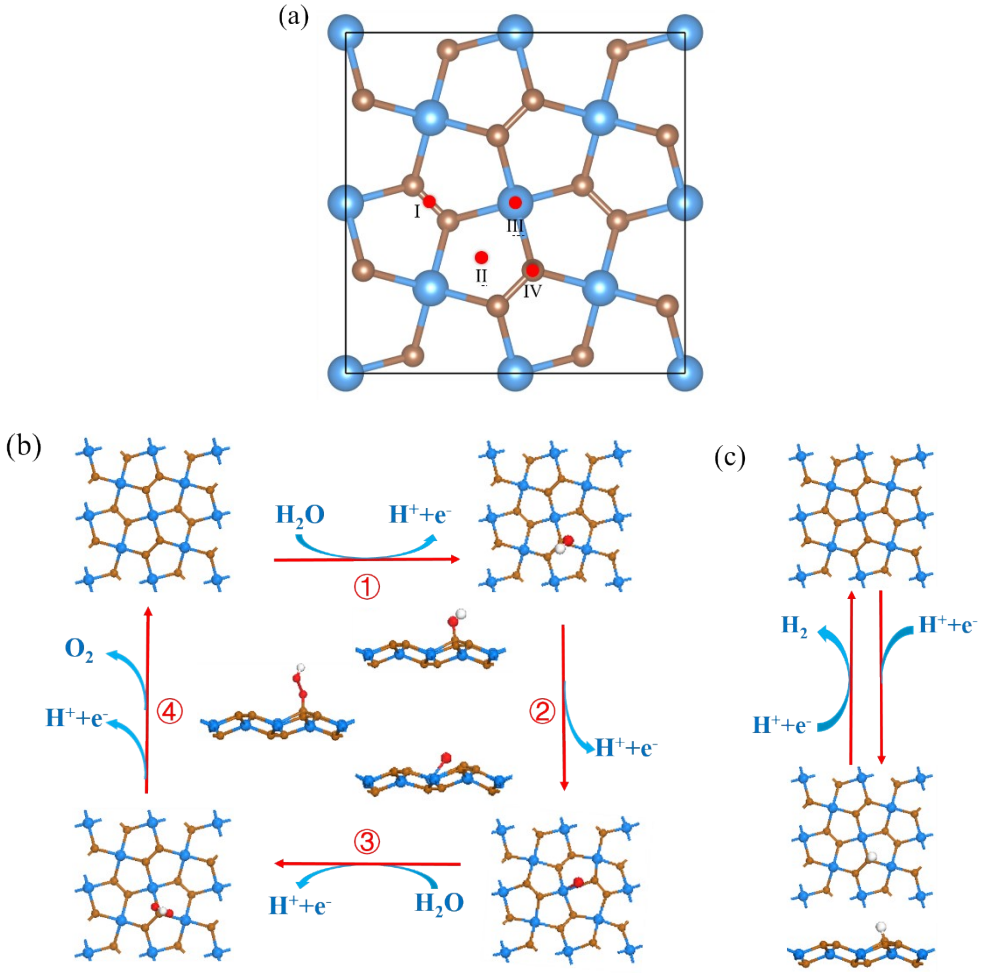

Fig. S5 (a) the intermediates adsorption sites at the *penta*-GeC_2 monolayer surface. (b) and (c) Proposed photocatalytic pathways of water oxidation and hydrogen reduction half-reactions with the most energetically favorable absorbed intermediates (OH*, O*, OOH*, and H*) in the *penta*-GeC_2 monolayer. The red and white balls represent O and H atoms, respectively.

Reference

[1] W. Zhang, C. C. Chai, Q. Y. Fan, M. L. Sun, Y. X. Song, Y. T. Yang, and U. Schwingenschlögl, *ACS Appl. Mat. & Inter.*, **2021**, 13, 14489-14496.

[2] X. Cai, Y. Chen, B. Sun, J. Chen, H. Wang, Y. Ni, L. Tao, H. Wang, S. Zhu, X. Li, Y. Wang, J. Lv, X. Feng, A.T. Redfern, and Z. Chen, Two-dimensional Blue-AsP Monolayers with Tunable Direct Band Gap and Ultrahigh Carrier Mobility Show Promising High performance Photovoltaic Properties, *Nanoscale*, **2019**, 10, 1039.

[3] S. Bruzzone and G. Fiori, Ab-initio simulations of deformation potentials and electron mobility in chemically modified graphene and two dimensional hexagonal boronnitride, *Appl. Phys. Lett.*, **2011**, 99, 222108.

[4] Y. Zhang, Y. Li, D. Ni, Z. Chen, X. Wang, Y. Bu, and J. Ao, Improvement of $BiVO_4$ Photoanode Performance During Water Photo-Oxidation Using Rh-Doped $SrTiO_3$ Perovskite as a Co-Catalyst, *Advanced Functional Materials*, **2019**, 29, 1902101.

[5] J. K. Nørskov, J. Rossmeisl, A. Logadottir, L. Lindqvist, J.R. Kitchin, T. Bligaard and H. Jónsson, Origin of the Overpotential for Oxygen Reduction at a Fuel-Cell Cathode. *J. Phys. Chem. B*, **2004**, 108, 17886.